Journal of Inorganic Biochemistry 130 (2014) 112–121

Contents lists available at ScienceDirect

Journal of Inorganic Biochemistry

journal homepage: www.elsevier.com/locate/jinorgbio

Searching for new aluminium chelating agents: A family of hydroxypyrone ligands

Leonardo Toso [a], Guido Crisponi [a], Valeria M. Nurchi [a,*], Miriam Crespo-Alonso [a], Joanna I. Lachowicz [a], Delara Mansoori [a], Massimiliano Arca [a], M. Amélia Santos [b], Sérgio M. Marques [b], Lurdes Gano [c], Juan Niclós-Gutíerrez [d], Josefa M. González-Pérez [d], Alicia Domínguez-Martín [d], Duane Choquesillo-Lazarte [e], Zbigniew Szewczuk [f]

[a] Dipartimento di Scienze Chimiche e Geologiche, Università di Cagliari, Cittadella Universitaria, 09042 Monserrato-Cagliari, Italy
[b] Centro Química Estrutural, Instituto Superior Técnico, Universidade Técnica de Lisboa, Av. Rovisco Pais, 1049-001 Lisboa, Portugal
[c] Campus Tecnológico e Nuclear, Instituto Superior Técnico, Universidade Técnica de Lisboa, Estrada Nacional 10, 2695-066 Bobadela LRS, Portugal
[d] Department of Inorganic Chemistry, Faculty of Pharmacy, Campus Cartuja, University of Granada, E-18071 Granada, Spain
[e] Laboratorio de Estudios Cristalográficos, IACT, CSIC-Universidad de Granada, Av. de las Palmeras 4, E-18100 Armilla, Granada, Spain
[f] Faculty of Chemistry, University of Wroclaw, F. Joliot-Curie 14, 50-383 Wroclaw, Poland

ARTICLE INFO

Article history:
Received 23 May 2013
Received in revised form 12 September 2013
Accepted 18 September 2013
Available online 18 October 2013

Keywords:
Aluminium related diseases
Chelation therapy
Kojic acid
Solution equilibria
Hydroxypyrones

ABSTRACT

Attention is devoted to the role of chelating agents in the treatment of aluminium related diseases. In fact, in spite of the efforts that have drastically reduced the occurrence of aluminium dialysis diseases, they so far constitute a cause of great medical concern. The use of chelating agents for iron and aluminium in different clinical applications has found increasing attention in the last thirty years. With the aim of designing new chelators, we synthesized a series of kojic acid derivatives containing two kojic units joined by different linkers. A huge advantage of these molecules is that they are cheap and easy to produce. Previous works on complex formation equilibria of a first group of these ligands with iron and aluminium highlighted extremely good pMe values and gave evidence of the ability to scavenge iron from inside cells. On these bases a second set of bis-kojic ligands, whose linkers between the kojic chelating moieties are differentiated both in terms of type and size, has been designed, synthesized and characterized. The aluminium^{III} complex formation equilibria studied by potentiometry, electrospray ionization mass spectroscopy (ESI-MS), quantum-mechanical calculations and ^{1}H NMR spectroscopy are here described and discussed, and the structural characterization of one of these new ligands is presented. The in vivo studies show that these new bis-kojic derivatives induce faster clearance from main organs as compared with the monomeric analog.

1. Introduction

Overviews on the pathological effects of aluminium overload in humans, and on its role in neurodegenerative diseases have been recently presented [1,2]. Aluminium was regarded as a non-toxic metal ion till the seventies of the last century, and its products have a number of applications, in medicine, in food processing, in water treatment, etc. The awareness that neurological and bone diseases in patients under dialysis treatment were related with aluminium toxicity encouraged the research on the management of aluminium intoxication. The reduction of all parenteral and oral aluminium exposures contributed to decrease aluminium dependent diseases in the last 20 years [3,4]. The aluminium chelation was recommended when patients did not clinically improve when aluminium exposure ceased [5]. Deferoxamine was the first aluminium chelator introduced in clinical practice that reduces not only bone aluminium deposit but also aluminium burden in the brain [6–12]. The acute neurological complications, which may be developed during Deferoxamine therapy for aluminium bone diseases, limited this treatment only to those patients with serum aluminium levels higher than 200 μg/L, or with aluminium bone concentration ten times greater than normal values [5,13,14]. Different aluminium chelators have been then introduced [15].

The aluminium chelation therapy has been founded on that in use for iron. Actually, massive research efforts due to the worldwide diffusion of iron overload diseases have lead to significant improvements in iron chelation. Evidence has been given for the utility, in aluminium dependent pathologies, of the knowledge acquired on iron chelating agents [16,17].

With the aim of designing new ligands that form high stability complexes, which satisfy the chemical and biological requirements for

* Corresponding author at: Dipartimento di Scienze Chimiche e Geologiche, Cittadella Universitaria, 09042 Monserrato-Cagliari, Italy. Tel.: +39 070 675 4476; fax: +39 070 675 4478.
E-mail address: nurchi@unica.it (V.M. Nurchi).

0162-0134/$ – see front matter © 2013 Elsevier Inc. All rights reserved.
http://dx.doi.org/10.1016/j.jinorgbio.2013.09.022

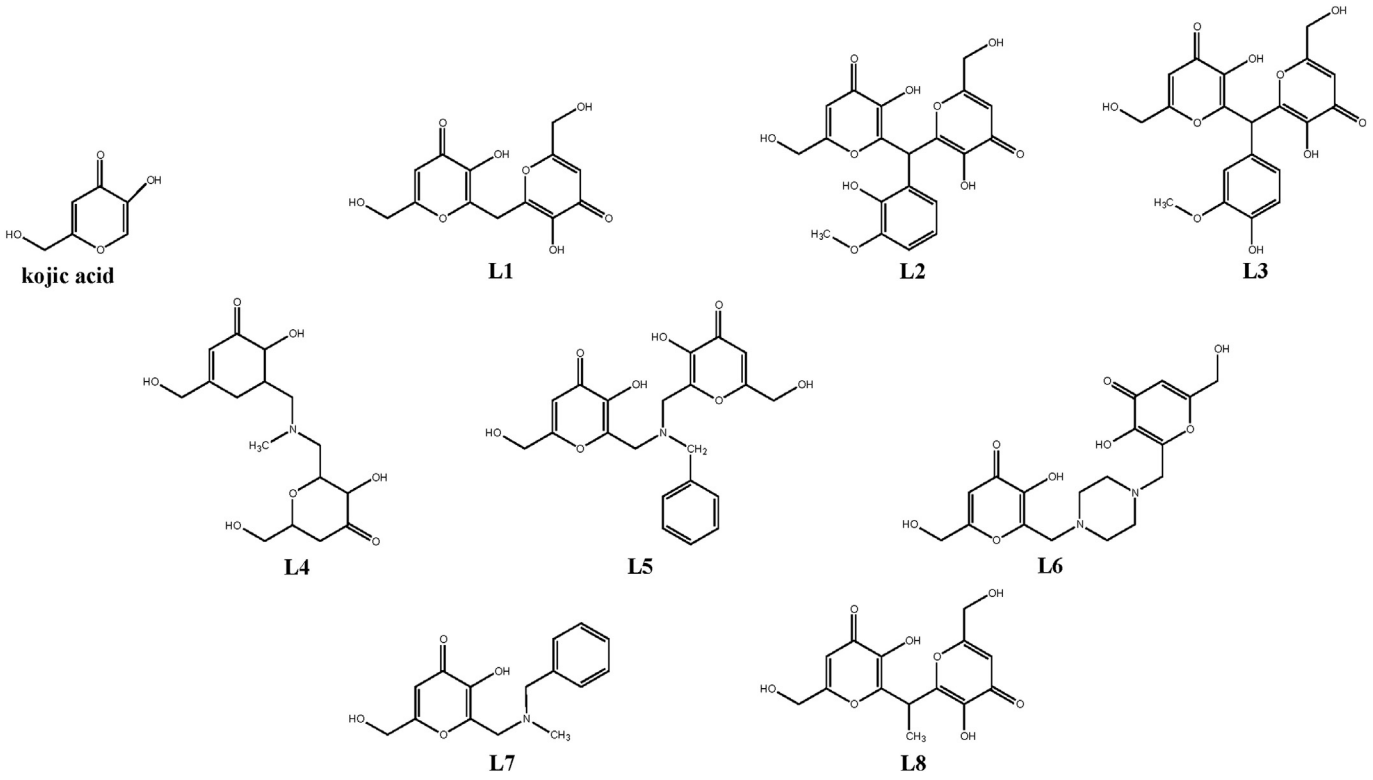

Scheme 1. Chemical structures and acronyms of studied ligands.

an effective chelating agent such as selectivity, lipophilicity and bioavailability, our group has synthesized some derivatives of kojic acid, and studied their complex formation equilibria with Fe^{III} and Al^{III}, as well as those with the parent ligand kojic acid (Scheme 1).

In previous works, the formation of MeL, MeL_2, and MeL_3 complexes of Al^{III} and Fe^{III} with kojic acid was remarked, and of diverse protonated species of Me_2L_2 and MeL_2 complexes with L1 [18], and with the related compounds in which vanillin and *o*-vanillin (L2 and L3) substituents were inserted on the linker [19]. The found pFe values (23.1 for L1, 18.9 for L2 and 22.2 for L3), lower than that for desferal (26.6) and comparable with that of deferiprone (20.7), and the fact that these ligands are easily and cheap to produce were very encouraging. We have recently synthesized a new set of bis-kojic ligands in which different linkers connecting the two kojic coordinating moieties have been designed for improving the interaction between the kojic units and the metal ions.

In this paper we will report the study on the complex formation equilibria of ligands L4–L8 as well as the structure characterization of L4 by X-ray diffraction. The in vivo efficacy of the ligands L4, L5, L7 and L8 as potential sequestering agents was also studied and reported herein, namely for the Ga-67 mobilization in mice previously injected with the radiotracer ^{67}Ga-citrate, as an animal model of Al-overload.

2. Experimental

2.1. Reagents

All the products, NaOH, KOH, and $AlCl_3$ purchased from Aldrich, HCl from Fluka, KCl from Carlo Erba (Milan, Italy), were used without further purification. An already described method was used for 0.1 M carbonate free KOH solution [20]. Ligand solutions were acidified with stoichiometric equivalents of HCl. Al^{III} solution was prepared by dissolving the required amount of $AlCl_3$ in pure double distilled water to which a stoichiometric amount of HCl was previously added to prevent hydrolysis. This solution was standardized by EDTA titration.

2.2. Synthesis

The synthesis of the ligands in Scheme 1 has been previously reported [21].

2.2.1. Synthesis of the L4 crystal

L4 (15 mg) was dissolved in distilled water (3 mL), aided by drop wise addition of HCl 0.01 M. Afterwards, isopropanol (3 mL) was added and the solution was left stirring for 30 min and then filtered into a crystallization device to remove possible impurities. The solution was placed into an acetone chamber diffusion, where acetone acts as antisolvent in crystallization process. After three weeks, parallelepiped colorless crystals appeared suitable for X-ray diffraction (XRD). It is also possible to obtain single crystals of L4 without acetone diffusion, leaving the solution to stand at room temperature. However, the quality of the crystals is lower, hence good quality data could not be obtained.

2.3. Potentiometric measurements

Potentiometric measurements of the complex formation equilibria were carried out under the same conditions described in a previous publication [18]. The operating ligand concentrations ranged from 3×10^{-4} to 3×10^{-3} M according to the examined ligand. The studies of complex formation were carried using constant ligand concentration, and 1:1, 1:2, and 1:3 metal/ligand molar ratios. To take into account the low complex formation rate with Al(III), a suitable procedure was used: the titrations started 1 h after the mixing of the reagents, long delay times between two subsequent additions were used (2–7 min) and the achievement of the equilibrium was checked using a drift parameter

of 1 mV/min [18]. Complex formation data were analyzed using the Hyperquad program [22].

2.4. ^{1}H NMR measurements

NMR spectra were recorded on a Bruker AVANCE III spectrometer at 300 MHz for ^{1}H NMR measurements. Chemical shifts (δ) are reported in ppm related to tetramethylsilane (TMS). The concentrations of the ligands ranged from 4 mM for L6 to 10 mM for L4, according to their solubility, and 1:3, 2:3 and 1:1 metal:ligand ratios were studied.

2.5. ESI-MS analysis of complexes

ESI-MS spectra were carried out on a Bruker microTOF-Q spectrometer (Bruker Daltonics, Bremen, Germany) equipped with an ESI source. Samples were dissolved in water and methanol 1:1 and the final pH was ~7. The ligand concentration was ~10^{-5} M and the ligand to metal molar ratio was 1:10. The experimental parameters were as follows: scan range 100–1600 *m/z*, drying gas nitrogen, temperature 200 °C, ion source voltage 4500 V, in-source collision energy 10 eV. The instrument operated in the positive ion mode and was calibrated externally with Tunemix™ mixture (Bruker Daltonics, Germany). Analyte solutions were introduced at a flow rate 3 μl/min. Compass Data Analysis (Bruker Daltonics, Germany) software was used to determine the formulae of the complexes. The stoichiometry of the complexes was unambiguously confirmed by distribution of the isotopic peaks and MS/MS analysis. The distance between the isotopic peaks allowed calculating the charge of the analyzed ions.

2.6. Crystal structure determination

Measured crystal was prepared under inert conditions immersed in perfluoropolyether as protecting oil for manipulation. Suitable crystals were mounted on MiTeGen Micromounts™ and these samples were used for data collection. Data were collected with Bruker SMART APEX (100 K) diffractometer. The data were processed with APEX2 [23] program and corrected for absorption using SADABS [24]. The structures were solved by direct methods, which revealed the position of all non-hydrogen atoms. These atoms were refined on F^2 by a full-matrix least-squares procedure using anisotropic displacement parameters [25]. All hydrogen atoms were located in difference Fourier maps and included as fixed contributions riding on attached atoms with isotropic thermal displacement parameters 1.2 times those of the respective atom. Geometric calculations were carried out with PLATON [26] and drawings were produced with PLATON and MERCURY [27]. Additional crystal data and more information about the X-ray structural analyses are shown in Supplementary material. Crystallographic data for the structural analysis have been deposited with the Cambridge Crystallographic Data Centre, CCDC 940707. Copies of this information may be obtained free of charge on application to CCDC, 12 Union Road, Cambridge CB2 1EZ, UK (fax: 44 1223 336 033; e-mail: deposit@ccdc.cam.ac.uk or http://www.ccdc.cam.ac.uk).

2.7. Theoretical calculations

Theoretical calculations were carried out on the ligands L4 and L6 in their neutral and *N*-protonated forms (see Results and discussion) and on the complexes $[Al_2(L4^-)_3]^{3+}$ and $[Al_2(L6)_3]^{6+}$ with the Gaussian09 (Rev. A.02) commercial suite of programs [28] at Density Functional Theory (DFT) level, adopting the mPW1PW91 (mPW1PW) functional by Adamo and Barone [29]. Schäfer, Horn, and Ahlrichs double-ζ plus polarization all-electron basis sets [30] were used for all atoms and were extracted from the Basis Set Exchange Database [31,32]. For each compound, the optimized geometries were verified through the calculations of harmonic vibrational frequencies computed analytically. Mulliken natural charges [33–35], and Wiberg bond indices [36] were calculated at the optimized geometries. The programs GaussView 5 and Molden 5.0 [37] were used to investigate the charge distributions and molecular orbital shapes. Calculations were carried out on a 64 bit E4 workstation equipped with four quad-core AMD Opteron processors and 16 Gb of RAM and running the Ubuntu 12.04 Linux OS and on a 64 bit IBM x3755 server equipped with four 12-core processors and 64 Gb of RAM running the SuSE 10.2 OS.

In order to estimate some pharmacokinetic parameters related with the ADME (absorption, distribution, metabolism and excretion) properties of the new compounds, a selection of molecular descriptors was calculated using Maestro 7.5 [38] and the corresponding QikProp program [39]. Maestro was used to build the molecular structure of the compounds which were energy minimized with Molten [37] and then re-imported by Maestro to run QikProp job. From the generated out-put file the following set of properties was predicted: the octanol/water partition coefficient (clog *P*), the aqueous solubility (log *S*, S in moles/L is the concentration of the solute in saturated solution), the apparent Caco-2 cell permeability in nm/s, the binding to Human serum albumin, the Human oral absorption in gastro-intestinal gut.

2.8. Biodistribution studies

^{67}Ga-citrate injection solution was prepared by dilution of ^{67}Ga-citrate from MDS Nordion with saline to obtain a final radioactive concentration of 5–10 MBq/100 μL. Biodistribution studies were carried out in groups of 3 female CD1 mice (randomly bred, Charles River, from CRIFFA, Barcelona, Spain) weighing *ca.* 25 g. Mice were intravenously (i.v.) injected with 100 μL (5–10 MBq) of ^{67}Ga-citrate via the tail vein immediately followed by intraperitoneal (i.p.) injection of 0.5 μmol of each ligand in 100 μL DMSO (L4, L5, L7) or saline (L8). L6 was not bioassayed due to its low solubility in water (neutral pH) or in DMSO. Animals were maintained on normal diet ad libitum and were sacrificed by cervical dislocation at 1 h and 24 h post-administration. The administered radioactive dose and the radioactivity in sacrificed animals were measured by a dose calibrator (Curiemeter IGC-3 Aloka, Japan). The difference between the radioactivity measured immediately after the injection and in the sacrificed animal, taking into account the radioactive decay was assumed to be due to whole body excretion. Tissue samples of main organs were then removed for counting in a gamma counter (Berthold LB2111, Berthold Technologies, Germany). Biodistribution results were expressed as percent of injected activity per total organ (% I.A./organ) and presented as mean values ± SD. For blood, bone and muscle, total activity was calculated assuming, as previously reported, that these organs constitute 7, 10 and 40% of the total weight, respectively. Statistical analysis of the data (*t*-test) was done with GraphPad Prism and the level of significance was set at 0.05.

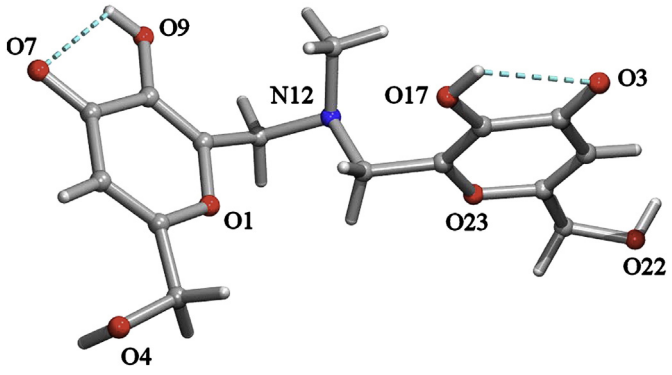

Fig. 1. Molecular structure of L4.

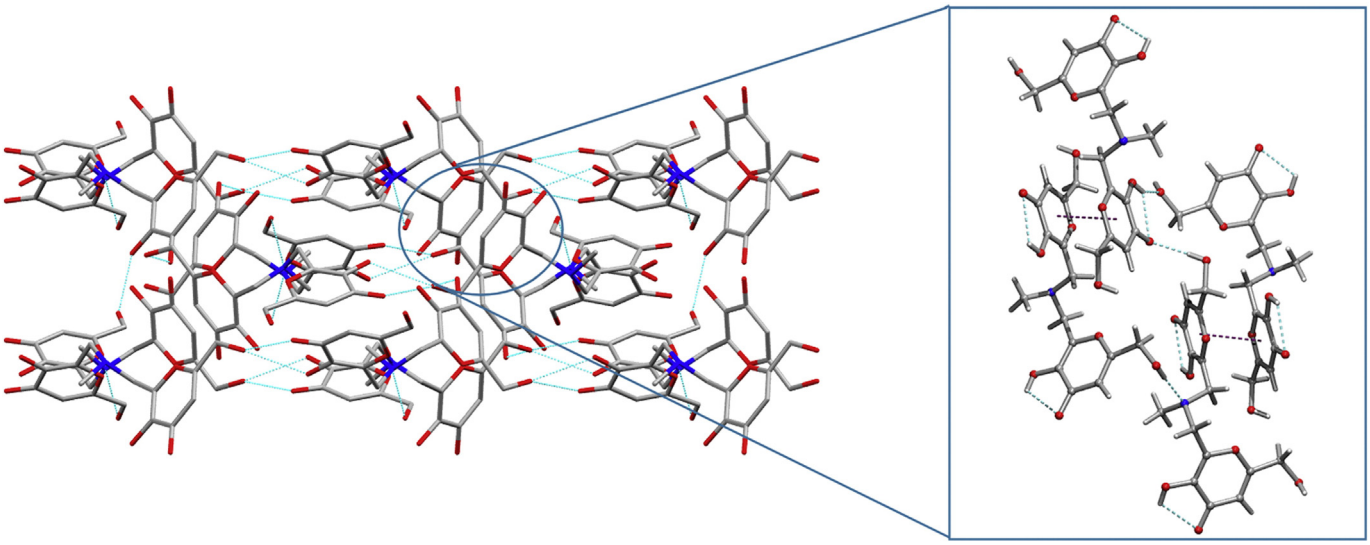

Fig. 2. Left: 3D architecture of the crystal of L4 with inter-molecular interactions (H-atoms omitted); right: detail of inter-molecular π,π-stacking interactions. Intra- and inter-molecular interactions are shown.

3. Results and discussion

3.1. Crystal structure of ligand L4

Ligand L4 crystallizes in the orthorhombic system, space group Pbca. The asymmetric unit consists of just one acid molecule (Fig. 1). The kojic acid moieties are stabilized by two intra-molecular H-bonding interactions involving the OH phenol-like groups as donors and the O keto-kojic groups as acceptors [O9–H···O7 (2.744(2) Å, 112.4°) and O17–H···O3 (2.797(2) Å, 111.3°)]. This feature has also been observed in closely related kojic-like compounds [19,21].

In the crystal of L4, adjacent acid molecules are linked via H-bonds with one OH-alcohol group and the quaternary N-atom being the H-donor and H-acceptor, respectively [O4–H···N12 (2.782(2) Å, 176.8°)]. These interactions build chains that extend along the *b* axis which are extra-stabilized by inter-molecular C–H···π interactions that involve the alcohol group and one kojic moiety [C3–H3A···Cg2 (2.74 Å, 160°)].[1] Neighboring chains are further connected by inter-molecular O–H(phenol-like)···O(alcohol) H-bonding interactions resulting in a 2D framework. Here the two kojic moieties within L4 are actively implicated [O9–H···O22 (2.854(2) Å, 164.7°) and O17–H···O4 (2.662(2) Å, 148.5°)]. The 3D architecture is accomplished by rather strong inter-molecular π,π-stacking [Cg2···Cg2 3.375 Å, $\alpha = 0°$, $\beta = \gamma = 16.13°$] and H-bonding interactions [(alcohol)O22–H···O3(keto-kojic) (2.801(2) Å, 173.6°)] (Fig. 2).

Interestingly, only one of the kojic moieties is involved in the referred π,π-stacking interactions. This mainly deals with the different torsion angles defined by the kojic moieties in the crystal [kojic#1: <N12–C11–C10–C8 107.42° or kojic#2: <N12–C14–C15–C16 95.61°].

3.2. Potentiometric and ^{1}H NMR results

The complex formation equilibria of all the five ligands with Al^{III} have been studied by potentiometric techniques (titration curves are provided in as supplementary material). At pH > 7 precipitation occurred, so the Hyperquad analysis was performed only on data before precipitation. The models and the relative complex formation constants are reported in Table 1, together with the protonation constants previously determined [21]. L4, L5 and L6 that are characterized by a longer linker than that of the previously studied L1, L2 and L3 ligands [19,21] form only one kind of complex of Al_2L_3 stoichiometry, variously protonated on the nitrogen atoms on the linker. As regard L4 and L5 ligands, the starting $Al_2L_3H_3$ species is the fully coordinated 2:3 complex with all the three protonated nitrogen atoms. L5, characterized by the piperazine ring in the linker, forms a starting $Al_2L_3H_4$ complex, in which one piperazine is protonated on both nitrogen atoms, while the other two only on a single one. These protons are lost at increasing pK values, with the same basicity order as in the free ligands L5 < L4 < L6.

L7 complexation scheme resembles that of the parent kojic acid with formation of AlL_2H_x complexes and, subsequently, an AlL_3 complex formed at higher pH than the corresponding complex with kojic acid. AlL_2H_2 is protonated on the nitrogen atom on the linkers. These protons are lost easier than in free ligand (pK = 6.0), their pK values being 5.52 and 5.64.

The last ligand L8 forms Al_2L_2 complexes of higher stability than those found with the analogous L1 ligand; the possibility of formation of Al_2L_3 complexes is counteracted by the too short linker. With respect to L1 complexes, the stronger stability of Al_2L_2 complexes prevents the formation of AlL_2 complexes. Estimation and comparison of these ligands as aluminium chelators can be done on the basis of the pAl values, reported in Table 1.

Table 1
Protonation and complex formation constants of the five ligands with Al^{III} at 25 °C, 0.1 M KCl ionic strength, obtained from potentiometric–spectrophotometric measurements.

Species	L4	L5	L6	L7	L8
LH	9.19 (3)	9.01 (2)	8.52 (4)	8.49 (1)	9.49 (2)
LH_2	16.70 (3)	16.62 (2)	16.66 (2)	14.51 (2)	16.18 (1)
LH_3	21.08 (5)	19.97 (2)	22.15 (5)		
LH_4			24.12 (5)		
Al_2L_2					31.99 (1)
$Al_2L_2H_{-1}$					27.10 (3)
$Al_2L_2H_{-2}$					21.71 (1)
$Al_2L_3H_4$	59.28 (4)		62.3 (1)		
$Al_2L_3H_3$	55.36 (5)	53.6 (1)	57.9 (3)		
$Al_2L_3H_2$	50.73 (5)	49.86 (8)	52.11 (2)		
Al_2L_3H	45.00 (5)	45.41 (7)	45.49 (1)		
Al_2L_3	37.4 (2)	37.9 (1)	37.73 (4)		
AlL_2H_2				27.53 (2)	
AlL_2H				22.01 (4)	
AlL_2				16.37 (3)	
AlL_3				21.39 (4)	
pAl	11.2	11.6	11.8	9.9	14.4

[1] Cg2 = centroid of the ring kojic#2: O(23)–C(15)–C(16)–C(18)–C(19)–C(20).

These pAl values, almost similar for L4, L5 and L6, in the range 11.1–11.8, characterize these ligands as less strong than L1, L2 and L3, with a shorter connecting chain between the two kojic moieties and with pAl values 12.8, 11.9 and 13.9, respectively. The potentiometric results are substantiated by the ^{1}H NMR spectra collected from solutions at different Al:L molar ratios and at variable pH from 1 to 10, whose behavior can be rationalized taking into account the speciation plots reported in Fig. 3.

As an example some illustrative ^{1}H NMR spectra collected on the system Al–L4 in the ratio 2:3 are reported in Fig. 4 together with the speciation plot of L4 and its aluminium complexes at the same 2:3 ratio. As the most representative protons of the system, the signals of H3 pyrone proton (6.6–7.4 ppm) and CH_3 on nitrogen atom (2.3–3.2 ppm) are reported in Fig. 4A. The bands at 6.60 ppm (H3) and at 3.15 ppm (CH_3) of free ligand are the only ones observed till pD 1.83. At pH 2.85 two new bands of the complexed ligand appear, one at 7.08 ppm of H3 proton, and the other at 2.94 ppm of CH_3 group. At pH 3.41 the intensity of these two bands increases with respect to those of free ligand, which completely disappear at pH 3.8. Just before pH 7 precipitation of the complex occurs. At basic pH values (>10.5) dissolution of complex takes place with formation of free ligand and of the soluble aluminium species $Al(OH)_4^-$.

Some considerations can be done on these behaviors:

- the slow exchange of ligand between its free and complexed form determines the appearance of separate NMR signals. One signal alone related to complexed ligand is observed, indicating the existence of only one kind of complex;
- no spectra of free ligand is present at pH > 3.80 for the NMR spectra collected on solutions at 2:3 Al:L4 molar ratios, differently from what happens in the spectra collected at 1:3 and 1:2 molar ratios. This strongly supports the existence of the unique $Al_2L_3H_x$ complex determined by potentiometric titrations;
- the signal of pyrone H3 in the complex is downfield shifted with respect to that in the free ligand, indicative of a deshielding action of aluminium complexation on the ring protons, while, the signal of CH_3 in the complex is not affected by that effect. On the contrary, there is a small shielding effect after starting the complex formation with respect to that in the free ligand. Thus, if there is any eventual minor deshielding effect of the Al^{III}, it might be overcome by some shielding effect due to an increase (ca. 0.4) on basicity of the nitrogen protons in the complexed forms with respect to that in the free ligand, due to the absence of hydrogen-bonding interaction with oxygen of OH chelating group;
- the stepwise deprotonation processes of ammonium protons of the aluminium complex seems responsible for a continuous shielding of the CH_3 signal, because of its adjacent positioning; as expected, the H3 signal is minimally affected by these deprotonations.

3.3. ESI-MS results

The ESI-MS spectra, collected for samples prepared at pH ~ 7, with a 10:1 metal excess, reveal further complexes not indicated by potentiometry and ^{1}H NMR spectroscopy. The ESI-MS spectrum of Al^{III}–L4 is presented in Fig. 5. The signal at *m/z* 364.047corresponds to $[L4_2Al_2]^{2+}$ complex formation, while the peak at 373.055 reveals a

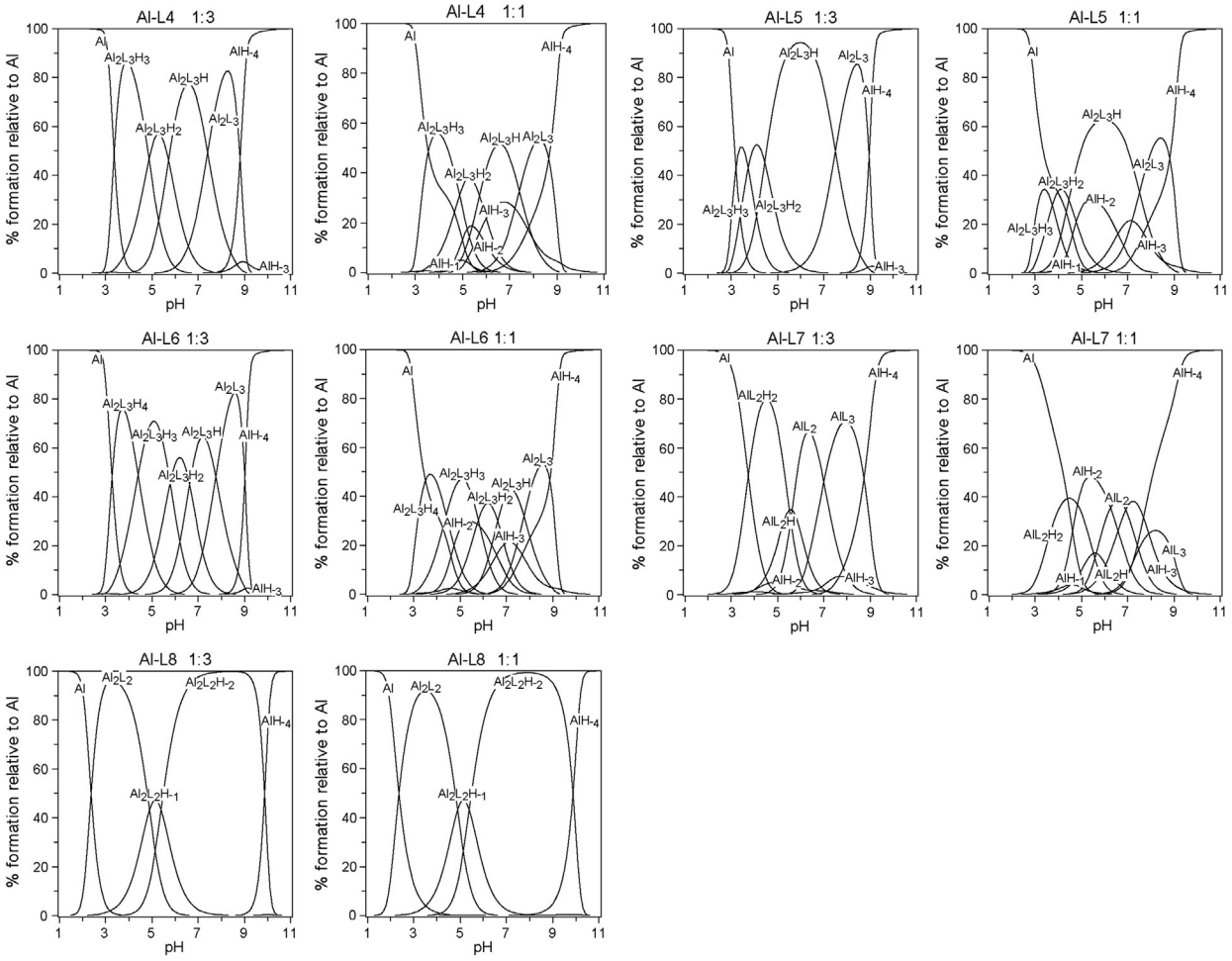

Fig. 3. Speciation plots of the systems Al^{III}–Ligands calculated with the stability constants in Table 1, at $[L] = 1.5 \times 10^{-3}$ M and $[Al^{III}] = 5 \times 10^{-4}$ M (1/3 plots) and 1.5×10^{-3} M (1/1 plots).

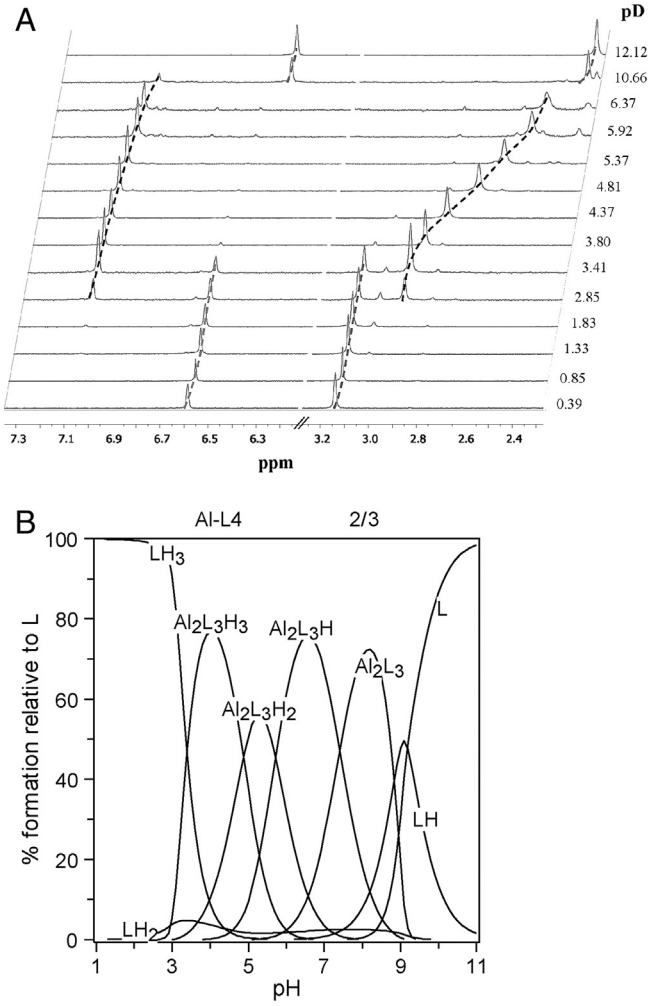

Fig. 4. A) ^{1}H NMR signals of H3 and of CH_3 of L4 at 2:3 aluminium ligand ratio; B) speciation plot of L4 at the same experimental condition.

hydrated $[L4_2Al_2 + H_2O]^{2+}$ complex. The peak corresponding to the free ligand is not present.

The ESI-MS spectrum in Fig. 6 displays the L5 complex formation with Al^{III} ions. The main peaks appear at *m/z* 416.128, *m/z* 432.101, *m/z* 440.086, *m/z*449.092 and *m/z* 458.093. The first peak at *m/z* 416.128 corresponds to the protonated free ligand. The peak at *m/z* 432.101 is indicative of the species $[L5_3Al_2]^{3+}$, visible also in experiments with higher metal ion excess. The peak at *m/z* 440.086 corresponds to the species $[L5_2Al_2]^{2+}$. The most abundant peak at *m/z* 449.092 and significantly less intense one at *m/z* 458.093 correspond to the mono-hydrated $[L5_2Al_2 + H_2O]^{2+}$ and bi-hydrated species $[L5_2Al_2 + 2H_2O]^{2+}$, respectively.

The representative ESI-MS spectrum of Al^{III} complexes with L6 is presented in Fig. 7. The highest intense peak at *m/z* 419.099 corresponds to the $[L6_2Al_2]^{2+}$ complex, while those with lower intensity, at *m/z* 428.103 and *m/z* 437.097, represent the mono-hydrated $[L6_2Al_2 + H_2O]^{2+}$ and bi-hydrated $[L6_2Al_2 + 2H_2O]^{2+}$ complexes, respectively.

3.4. QM-calculations

During the past decades, quantum-mechanical (QM) calculations have gained an increasing interest due to their ability to help the investigations on the structural, spectroscopic, and electrochemical features of inorganic and organometallic compounds. In recent years, density functional theory (DFT) [40–42] has been widely recognized as a theoretical tool capable of providing very accurate information at an acceptable computational cost.

Recently, some of the authors exploited DFT calculations to investigate the relative stabilities of Al^{III} and Fe^{III} complexes featuring the 2,2′-[(2-hydroxy-3-methoxyphenyl)methanediyl]bis[3-hydroxy-6-(hydroxyl methyl)-4*H*-pyran-4-one] and 2,2′-[(4-hydroxy-3-methoxyphenyl)methanediyl] bis[3-hydroxy-6-(hydroxyl methyl)-4*H*-pyran-4-one] ligands [19].

Prompted by these results, DFT calculations have been extended to the ligands L4 and L6, featuring two kojic residues separated by spacers capable of providing them the ability to form binuclear monomeric complexes. With the aim to validate the computational

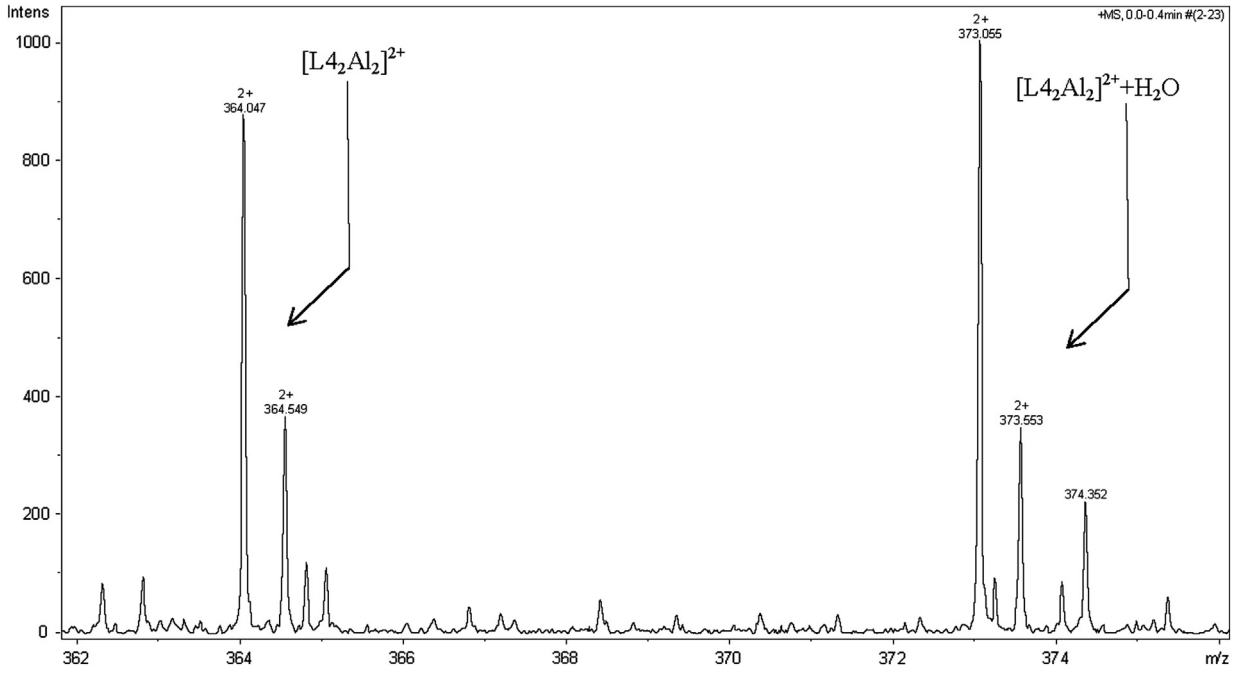

Fig. 5. ESI-MS spectrum of Al^{III}–L4 complexes.

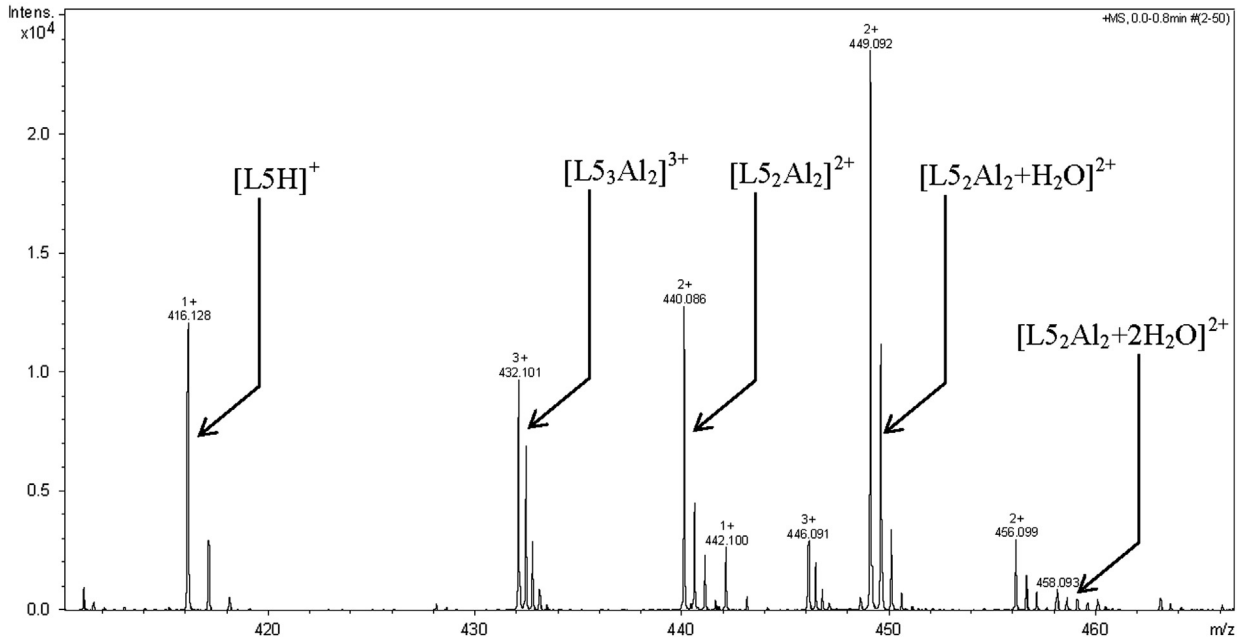

Fig. 6. ESI-MS spectrum of Al^{III}–L5 complexes.

set-up, the metric parameters optimized for the neutral form of L4 have been compared with the corresponding ones determined by X-ray diffraction (see above). In agreement with diffractometric data, the hydroxyl groups of the kojic units are involved in H-bonding interactions with the adjacent carbonyl groups (O–H···O 2.587 Å, 121.7°). The localization of Kohn–Sham (KS) HOMO (Highest-Occupied Molecular Orbital) on the quaternary N atom accounts both for its basicity in solution and for its ability to participate to inter-molecular H-bonding interactions.

In order to verify the donor ability of the ligands in acidic media, both ligands have been studied in their *N*-protonated forms ($L4^-$ and L6, respectively), with the deprotonated oxygen donor atoms belonging to the kojic acid moieties. In the case of $L4^-$, the geometry optimization occurred through a proton transfer from the nitrogen atom to one of the two kojic oxygen donor atoms. The resulting optimized structure is stabilized by an O–H···O hydrogen bond linking the two kojic residues. On the contrary, in the case of L6, optimized with the piperazine spacer disposed in a chair configuration, such stabilization did not occur and therefore the optimization of the *N*-protonated species is feasible. The optimized structure of L6 displays metric parameters close to those previously calculated for related systems [19]. In particular, the two C–O distances of each donor groups show significantly different distances (1.217 and 1.262 Å, respectively), reflected in different Wiberg bond indices [36] (average value 1.681 and 1.373, respectively).

Filled molecular orbitals can be found localized on the oxygen atoms of the kojic residues. In particular, the couples HOMO-3/HOMO-2 and

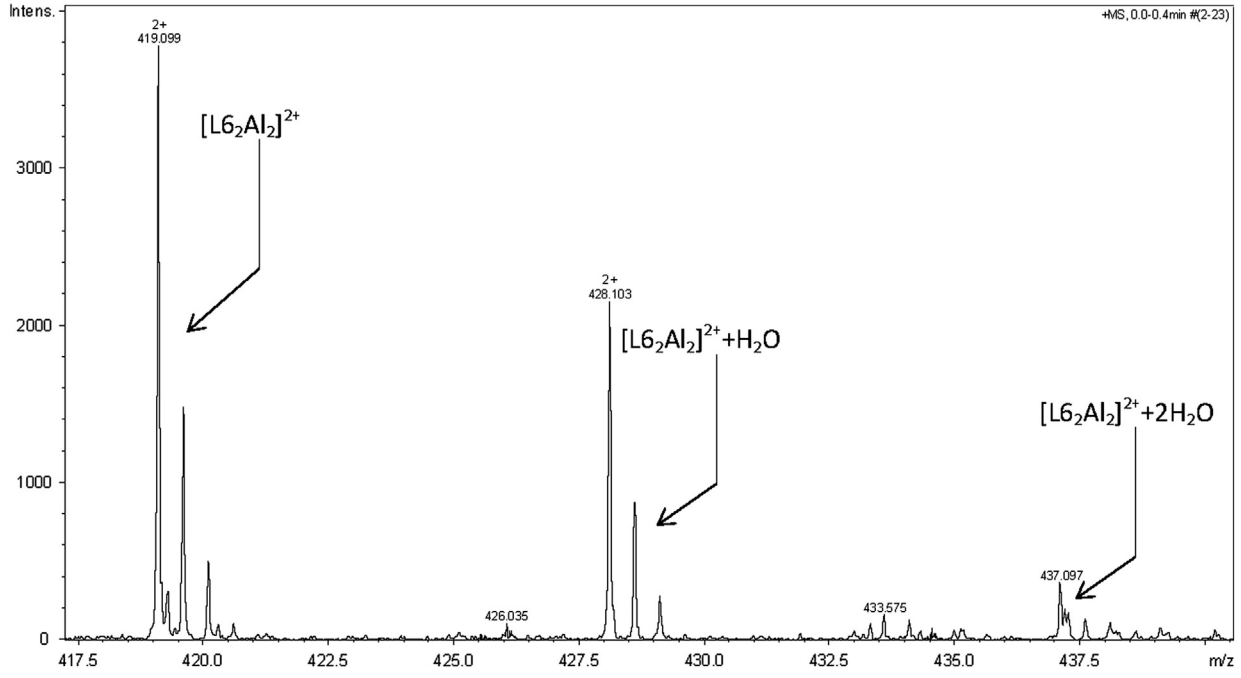

Fig. 7. ESI-MS spectrum of Al^{III}–L6 complexes.

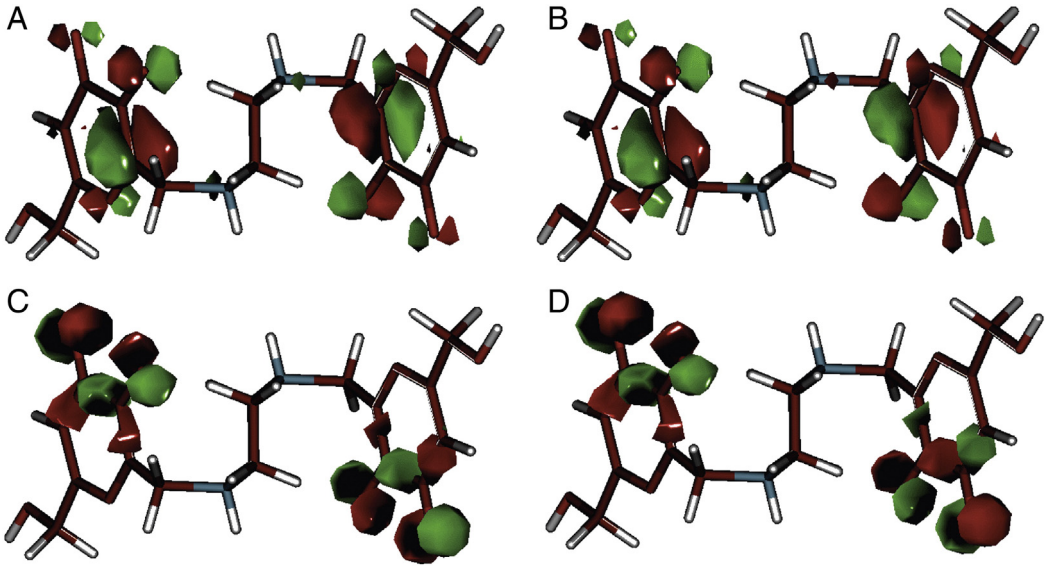

Fig. 8. Drawings of the isosurfaces of Kohn–Sham HOMO (A), HOMO-1 (B), HOMO-2 (C) and HOMO-3 (D) calculated for L6. Contour value 0.05 e.

HOMO-1/HOMO exhibit large contributions from the symmetric and antisymmetric combinations of the 2*p* oxygen atomic orbitals laying on the plane of the 4*H*-pyran-4-one ring and perpendicularly to it, respectively (Fig. 8), which feature remarkable negative natural charges (−0.575 and −0.769 e), being therefore available to coordinate the Al^{III} centers.

Based on potentiometric and ^{1}H-NMR measurements, the complexes featuring 2:3 metal:ligand ratios were also optimized for the two ligands. In the binuclear cation $[Al_2(L4^{-})_2]^{3+}$ (corresponding to the $Al_2L_3H_3$ stoichiometry discussed above and identified in solution above pH 3.9) the optimised Al···Al distance was calculated to be 6.084 Å. Each Al^{III} is coordinated in a distorted octahedral fashion by the oxygen atoms from three deprotonated kojic acid units of different ligands (Fig. 9).

In each kojic unit, the two optimized C–O distances and the corresponding Al–O are statistically different, with average C–O distances of 1.257(1) and 1.291(6) Å and Al–O distances of 1.897(9) and 1.95(1) Å [average 1.92(3) Å]. The complex is stabilized by three hydrogen bonds established between the N–H group of the protonated spacers and the hydroxyl groups of the hydroxymethyl substituents of each 4*H*-pyrane ring.

The structure of $[Al_2(L6)_3]^{6+}$ shows very similar structural features. The different nature of the spacer between the two kojic residues in each ligand unit results in a larger separation between the two Al^{III} centers (8.091 Å) and also in this case the two C–O bonds within each donor unit feature different distances [1.260(4) and 1.31(2) Å; average Al–O distance 1.93(3) Å].

Finally, an examination of the net positive charge on the metal centers calculated at NBO level (1.999 and 2.003 e for $[Al_2(L4^{-})_2]^{3+}$ and $[Al_2(L6)_3]^{6+}$, respectively) testifies for the very polarized nature of Al–O bonds in both compounds, which is independent on the global charges of the two complexes.

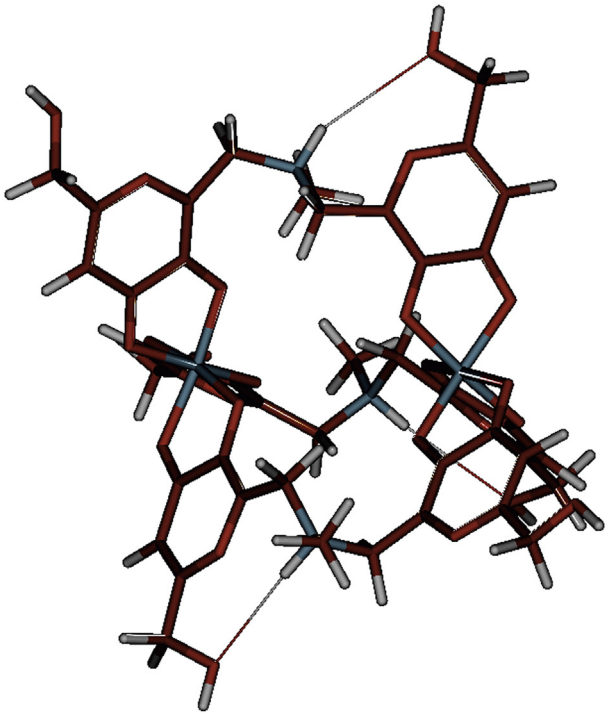

Fig. 9. Drawing of the optimized structure of the complex $[Al_2(L4^{-})_3]^{3+}$.

3.5. Biodistribution studies

To evaluate the efficacy of the new ligands L4, L5, L7 and L8, as chelating agents for mobilization of metal ions, we studied their effect on the usual biodistribution profile of the well-established ^{67}Ga-citrate in female mice after intravenous administration of the radiotracer. The tissue distribution of this radiotracer was compared to its distribution with simultaneous intraperitoneal administration of 0.5 μmol of each ligand solution.

The effect of this series of chelators on the ^{67}Ga uptake and clearance on the major organs and on the excretion, in comparison with that of the ^{67}Ga-citrate, can be overviewed graphically in Fig. 10 as well as in Table 2. The influence of the commercially available iron-chelating drug, deferiprone (DFP), previously evaluated in the same animal model [43], was also included in this graphic presentation.

Analysis of these results shows that the co-administration of the ligands interferes in the usual tissue distribution of the radioactive metal in mice enhancing the overall excretion rate of radioactivity from whole animal body. The four ligands can induce modifications on the ^{67}Ga biodistribution pattern with the same trend, enhancement of its total excretion. No significant differences in the rate of radioactivity elimination were found, except by administration of L7 that induced a slower excretion. The most important differences in the distribution profile are related with the blood clearance. L7 and L8 induce slower clearance from blood than the other two compounds, at 1 h after administration, which may be attributed to a highest level of plasmatic

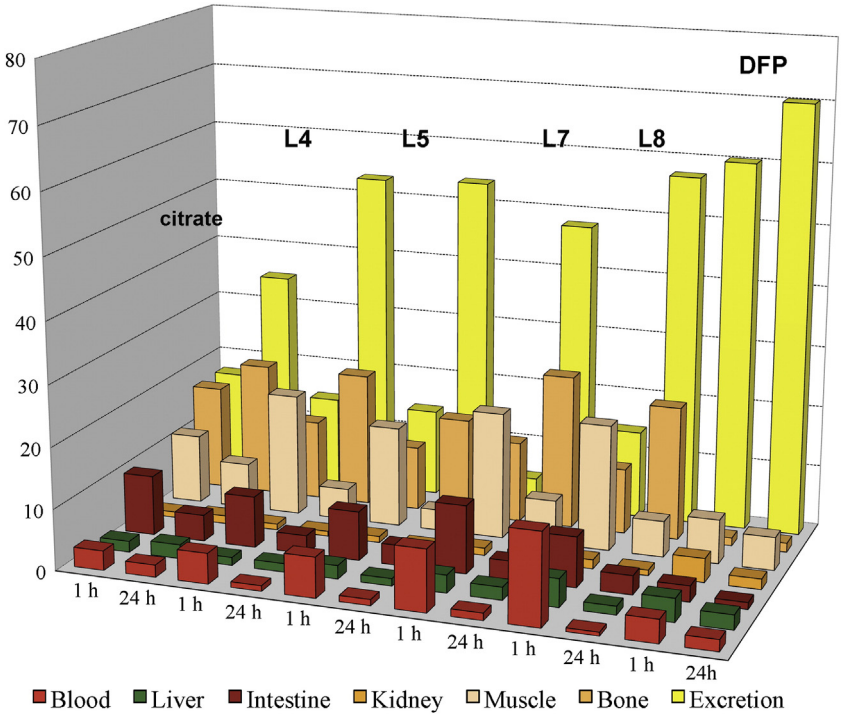

Fig. 10. Biodistribution data in the most relevant organs, expressed as % I.A./organ for ^{67}Ga-citrate (i.v. injection) and ^{67}Ga-citrate with simultaneous intraperitoneal injection of the ligands L4, L5, L7, L8 and DFP [43], at 1 and 24 h after intravenous administration in female mice (n = 3–5).

protein binding. Consequently highly irrigated organs like the heart, lungs and kidneys also present the highest radioactivity levels.

This improvement in the elimination rate of the radiotracer makes evident the ability of the ligands to coordinate in vivo with gallium, suggesting their potential as decorporating agent of this metal. However, high levels of radioactivity are retained in the muscle and bone tissues which are similar to those of the radiotracer. Comparison of our data with those of DFP indicates that the drug is able to induce the fastest clearance from organs like muscle and bone and total excretion.

Some rationalization of these bioassays can be aided by different parameters, namely the metal chelating ability of the compounds and the pharmacokinetic properties of the ligands and corresponding metal complexes. Since it is known that the Al(III) and Ga(III) chelating ability of analogous hard ligands follows a parallel trend [43,44], on the basis of the calculated pAl values (Table 1) it can be anticipated that L4 and L5 present an identical gallium chelating capacity (pAl = 11.2–11.6) while L7 and L8 present the lowest (pAl = 9.9) and the highest (pAl = 14.4) values, respectively (DFP presents the highest value (pAl = 16.0) [43], due to its different *N*-heterocyclic nature). Interestingly, an identical trend was found for the total metal excretion at 24 h. Further differences on the biodistribution profile could also be partially rationalized on the basis of the predicted values for some of the pharmacokinetic properties for ligands and complexes, namely lipophilicity, membrane crossing ability, binding with serum proteins. However, the calculated ligand descriptors (see Table 3) [38,39] did not allow a good rationalization match. In particular, although the monochelators L7 and DFP present quite good similarities on some estimated properties (molecular weight, lipophilicity, interaction with human serum albumin (HAS), gastro-intestinal (GI) absorption), considerable differences found on membrane

Table 2
Biodistribution data at the most relevant organs, expressed as % I.A./organ for ^{67}Ga-citrate with simultaneous intraperitoneal injection of the ligands L4, L5, L7, L8 at 1 h and 24 h, after intravenous administration in female mice (n = 3).

Organs	I.A./organ (%)							
	L4		L5		L7		L8	
	1 h	24 h	1 h	24 h	1 h	24 h	1 h	24 h
Blood	5.0 ± 0.8	0.9 ± 0.5	6.6 ± 2.6	1.0 ± 0.4	10.1 ± 2.6*	1.2 ± 0.6	15.0 ± 4.6*	0.6 ± 0.1
Liver	1.3 ± 0.4*	1.4 ± 0.4	2.2 ± 0.3	1.2 ± 0.2	2.9 ± 0.8	2.1 ± 0.3	4.6 ± 0.4*	1.4 ± 0.5
Intestine	8.4 ± 0.8	3.0 ± 0.7	8.0 ± 1.5	3.3 ± 0.2	11.1 ± 0.7*	3.0 ± 0.2	8.2 ± 1.8	3.1 ± 1.3
Spleen	0.07 ± 0.01	0.06 ± 0.03	0.11 ± 0.06	0.05 ± 0.02	0.2 ± 0.06	0.06 ± 0.01	0.22 ± 0.09*	0.08 ± 0.04
Heart	0.20 ± 0.02	0.08 ± 0.05	0.28 ± 0.05	0.06 ± 0.01	0.4 ± 0.1*	0.07 ± 0.03	0.4 ± 0.2*	0.06 ± 0.03
Lung	0.44 ± 0.03	0.14 ± 0.03	0.6 ± 0.2	0.09 ± 0.05	1.3 ± 0.5*	0.2 ± 0.1	1.0 ± 0.3	0.18 ± 0.08
Kidney	0.97 ± 0.03	0.8 ± 0.1	1.0 ± 0.1	0.5 ± 0.1	1.2 ± 0.2	1.5 ± 0.2	1.47 ± 0.04*	0.9 ± 0.1
Muscle	20.0 ± 4.6	5.10 ± 0.04	16.4 ± 1.1	3.4 ± 1.1	20.7 ± 1.4	7.2 ± 1.0	20.6 ± 2.4	5.9 ± 0.4
Bone	13.0 ± 0.8	21.9 ± 2.5	10.5 ± 1.0*	16.1 ± 1.6*	13.2 ± 0.6	25.2 ± 2.6	10.7 ± 0.2	21.9 ± 1.4
Stomach	0.97 ± 0.05	0.7 ± 0.3	0.8 ± 0.1	0.6 ± 0.1	0.72 ± 0.01	0.4 ± 0.1	0.7 ± 0.1	0.45 ± 0.05
Brain	0.06 ± 0.01	0.02 ± 0.01	0.05 ± 0.01	0.02 ± 0.01	0.13 ± 0.04	0.02 ± 0.00	0.12 ± 0.05	0.02 ± 0.01
Excretion	14.5 ± 1.3	53.3 ± 4.8	14.2 ± 2.4	53.9 ± 2.9	4.4 ± 0.1*	48.0 ± 4.0	14.3 ± 4.8	57.4 ± 5.6

* $p < 0.05$.

Table 3
Predicted pharmacokinetic properties for the ligands.[a]

	MW	clog P[b]	log S[c] (H_2O)	Caco-2 permeability (nm/s)	Log K[d] (HSA)	H oral absorption in GI (%)[e]
L4	339	−1.567	−0.714	6	−1.018	38
L5	415	−0.351	−0.947	8	−0.726	49
L6	394	−2.055	−0.072	1	−1.021	34
L7	275	0.685	−1.081	95	−0.475	75
L8	310	−0.887	−2.029	24	−0.838	37
DFP	139	0.655	−1.334	1024	−0.539	79

[a] Predicted values using program QikProp v. 2.5 [39].
[b] Octanol/water partition coefficient.
[c] Aqueous solubility.
[d] Binding Human serum albumin.
[e] % of Human oral absorption in gastro-intestinal gut.

permeability and chelating capacity may have account for L7 coming out with the lowest metal excretion capability and concomitant highest retention in bone, intestine and muscles, in opposition to DFP. The ligands containing two kojic units (L4, L5 and L8) present a similar in vivo behavior at 1 h (despite the slowest blood clearance induced by L8), while at 24 h, L8 appears as the most efficient metal mobilizing ligand, eventually due to both the higher chelating affinity and more favorable efflux properties of its smaller metal complex.

4. Conclusions

The complex formation equilibria of aluminium^{III} with five new ligands recently synthesized and structurally characterized have been studied by potentiometry and ^{1}H NMR spectra. Complementary supporting information has been obtained from ESI-MS spectroscopy and quantum-mechanical calculations. The complex formation equilibria of L4, L5 and L6 with Al^{III} are characterized by the formation of a 2:3 Al:L complex variously protonated, as the major species, in the whole pH range. L7 is characterized by the formation of 1:2 and 1:3 Al:L complexes, as the parent ligand kojic acid. Instead, L8 forms a 2:2 Al:L complex which is stabilized at high pH values by the formation of mixed hydroxo complexes. The pAl values of these ligands (Table 1) allow to remark the very good chelating qualities of ligand L8 (14.4), superior to that of the analogous L1 ligand (12.8). The remaining ligands L4–L6, containing nitrogen atoms in the linker, show a minor chelating efficiency, the pAl ranging from 11.1 for L4 to 11.8 for L6, while L7 that contains only one kojic residue is characterized by the lowest pAl (9.9). The high efficiency of this family of ligands with respect to the simple parent kojic acid is strongly determined by the complete involvement of the second kojic unit through the formation of dinuclear aluminium complexes in which each of the two aluminium ions is coordinated by two or three kojic chelating moieties. Studies in mice confirmed the high in vivo metal sequestering power of the bischelators, in comparison with the corresponding monochelator. The excellent chelating properties recommend further toxicological and pharmacological research on these new promising ligands.

Acknowledgments

GC and JIL acknowledge Regione Sardegna for the financial support CRP-27564, project “Integrated approach in the design of chelators for the treatment of metal overload diseases”. MCA is grateful to RAS for the program Master and Back — Percorsi di rientro, PRR-MAB-A2011-19107. MAS acknowledge FCT for financial support, project PEst-OE/QUI/UI0100/2011.

Appendix A. Supplementary data

Supplementary data to this article can be found online at http://dx.doi.org/10.1016/j.jinorgbio.2013.09.022.

References

[1] G. Crisponi, V.M. Nurchi, G. Faa, M. Remelli, Monatsh. Chem. 142 (2011) 331–340.
[2] G. Crisponi, V.M. Nurchi, V. Bertolasi, M. Remelli, G. Faa, Coord. Chem. Rev. 256 (2012) 89–104.
[3] M.D. Arenas Jiménez, T. Malek, M.T. Gil, A. Moledous, C. Núñez, F. Álvarez-Ude, Nefrologia 28 (2008) 168–173.
[4] H. Graf, H.K. Stummvoll, V. Meisinger, J. Kovarik, A. Wolf, W.F. Pinggera, Kidney Int. 19 (1981) 587–592.
[5] A.C. Alfrey, in: M. Nicolini, P.F. Zatta, B. Corain (Eds.), Aluminium in Chemistry, Biology and Medicine, Cortina International Verona and Raven Press, New York, 1991, pp. 73–84.
[6] R.A. Yokel, P. Ackrill, E. Burgess, J.P. Day, J.L. Domingo, T.P. Flaten, J. Savory, J. Toxicol. Environ. Health 48 (1996) 667–683.
[7] H.G. Nebeker, D.S. Milliner, S.M. Ott, D.J. Sherrard, A.C. Alfrey, J.G. Abuelo, A. Wasserstein, Kidney Int. 25 (1984) 173–180.
[8] C. Ciancioni, J.L. Poignet, C. Naret, S. Delons, Y. Mauras, P. Allain, N.K. Man, Proc. Eur. Dial. Transplant. Assoc. Eur. Ren. Assoc. 21 (1985) 469–473.
[9] B.A. Molitoris, P.S. Alfrey, N.L. Miller, J.A. Hasbargen, W.D. Kaehney, B.J. Smith, Kidney Int. 31 (1987) 986–991.
[10] D.J. Brown, J.K. Dawborn, K.N. Ham, J.M. Xipell, Lancet 2 (1982) 343–345.
[11] R.A. Yokel, S.S. Rhineheimer, P. Sharma, D. Elmore, P.J. McNamara, Toxicol. Sci. 64 (2001) 77–82.
[12] H. Nakamura, P.G. Rose, J.L. Blumer, M.D. Reed, J. Clin. Pharmacol. 40 (2000) 296–300.
[13] D.J. Sherrard, J.V. Walker, J.L. Boykin, Am. J. Kidney Dis. 12 (1988) 126–130.
[14] S. Ghitu, R. Oprisiu, L. Benamar, S. Said, A.T. Albu, I. Arsenescu, N. El Esper, P. Morinière, A. Fournier, Ostéodystrophie rénale (3); son traitement chez le dialysé, 21 (2000) 413–424.
[15] T.P. Kruck, J.G. Cui, M.E. Percy, W.J. Lukiw, Cell. Mol. Neurobiol. 24 (2004) 443–459.
[16] G. Crisponi, V.M. Nurchi, J. Inorg. Biochem. 105 (2011) 1518–1522.
[17] M.A. Santos, M.A. Esteves, S. Chaves, Curr. Med. Chem. 19 (2012) 2773–2793.
[18] V.M. Nurchi, G. Crisponi, J.I. Lachowicz, S. Murgia, T. Pivetta, M. Remelli, A. Rescigno, J. Niclós-Gutíerrez, J.M. González-Pérez, A. Domínguez-Martín, A. Castiñeiras, Z. Szewczuk, J. Inorg. Biochem. 104 (2010) 560–569.
[19] V.M. Nurchi, J.I. Lachowicz, G. Crisponi, S. Murgia, M. Arca, A. Pintus, P. Gans, J. Niclos-Gutierrez, A. Domínguez-Martín, A. Castineiras, M. Remelli, Z. Szewczuk, T. Lis, Dalton Trans. 40 (2011) 5984–5998.
[20] V.M. Nurchi, G. Crisponi, M. Crespo-Alonso, J.I. Lachowicz, Z. Szewczuk, G.J.S. Cooper, Dalton Trans. 42 (2013) 6161–6170.
[21] L. Toso, G. Crisponi, V.M. Nurchi, M. Crespo-Alonso, J.I. Lachowicz, M.A. Santos, S.M. Marques, J. Niclos-Gutierrez, J.M. Gonzalez-Perez, A. Dominguez-Martin, D. Choquesillo-Lazarte, Z.Z. Szewczuk, J. Inorg. Biochem. 227 (2013) 220–231, http://dx.doi.org/10.1016/j.jinorgbio.2013.06.009.
[22] P. Gans, A. Sabatini, A. Vacca, Talanta 43 (1996) 1739–1753.
[23] APEX2 Software, Bruker AXS Inc. v2010.3-0, 2010. (Madison, Wisconsin, USA).
[24] G.M. Sheldrick, SADABS, Program for Empirical Absorption Correction of Area Detector Data, University of Gottingen, Germany, 2009.
[25] G.M. Sheldrick, Acta Crystallogr. A 64 (2007) 112–122.
[26] A.L. Spek, Utrecht University, Utrecht, The Netherlands, 2010.
[27] C.F. Macrae, I.J. Bruno, J.A. Chisholm, P.R. Edgington, P. McCabe, E. Pidcock, L. Rodriguez-Monge, R. Taylor, J. Van De Streek, P.A. Wood, J. Appl. Crystallogr. 41 (2008) 466–470.
[28] M.J. Frisch, G.W. Trucks, H.B. Schlegel, G.E. Scuseria, M.A. Robb, J.R. Cheeseman, G. Scalmani, V. Barone, B. Mennucci, G.A. Petersson, H. Nakatsuji, M. Caricato, X. Li, H.P. Hratchian, A.F. Izmaylov, J. Bloino, G. Zheng, J.L. Sonnenberg, M. Hada, M. Ehara, K. Toyota, R. Fukuda, J. Hasegawa, M. Ishida, T. Nakajima, Y. Honda, O. Kitao, H. Nakai, T. Vreven, J. Montgomery, J. A., J.E. Peralta, F. Ogliaro, M. Bearpark, J.J. Heyd, E. Brothers, K.N. Kudin, V.N. Staroverov, R. Kobayashi, J. Normand, K. Raghavachari, A. Rendell, J.C. Burant, S.S. Iyengar, J. Tomasi, M. Cossi, N. Rega, J.M. Millam, M. Klene, J.E. Knox, J.B. Cross, V. Bakken, C. Adamo, J. Jaramillo, R. Gomperts, R.E. Stratmann, O. Yazyev, A.J. Austin, R. Cammi, C. Pomelli, J.W. Ochterski, R.L. Martin, K. Morokuma, V.G. Zakrzewski, G.A. Voth, P. Salvador, J.J. Dannenberg, S. Dapprich, A.D. Daniels, Ö. Farkas, J.B. Foresman, J.V. Ortiz, J. Cioslowski, D.J. Fox, Gaussian 09, Revision A.1, 2009.
[29] C. Adamo, V. Barone, J. Chem. Phys. 108 (1998) 664–675.
[30] A. Schäfer, H. Horn, R. Ahlrichs, J. Chem. Phys. 97 (1992) 2571–2577.
[31] D. Feller, J. Comput. Chem. 17 (1996) 1571–1586.
[32] K.L. Schuchardt, B.T. Didier, T. Elsethagen, L. Sun, V. Gurumoorthi, J. Chase, J. Li, T.L. Windus, J. Chem. Inf. Model. 47 (2007) 1045–1052.
[33] E.D. Glending, C.R. Landis, F. Weinhold, NBO Version 3.1, 1996.
[34] A.E. Reed, F. Weinhold, J. Chem. Phys. 83 (1985) 1736–1740.
[35] A.E. Reed, R.B. Weinstock, F. Weinhold, J. Chem. Phys. 83 (1985) 735–746.
[36] K.B. Wiberg, Tetrahedron 24 (1968) 1083–1096.
[37] G. Schaftenaar, J.H. Noordik, J. Comput. Aided Mol. Des. 14 (2000) 123–134.
[38] Maestro, Version 7.5, Schrödinger Inc., Portland, OR, 2005.
[39] QikProp, Version 2.5, LCC, New York, NY, 2005.
[40] W. Koch, M.C. Holthausen, Front Matter and Index, Wiley-VCH Verlag GmbH, 2001. 1–13.
[41] C.J. Cramer, D.G. Truhlar, PCCP 11 (2009) 10757–10816.
[42] E.R. Davidson, Chem. Rev. 100 (2000) 351–352.
[43] S. Chaves, A. Capelo, L. Areias, S.M. Marques, L. Gano, M.A. Esteves, M.A. Santos, Dalton Trans. 42 (2013) 6033–6045.
[44] R. Grazina, L. Gano, J. Šebestík, M. Amelia Santos, J. Inorg. Biochem. 103 (2009) 262–273.